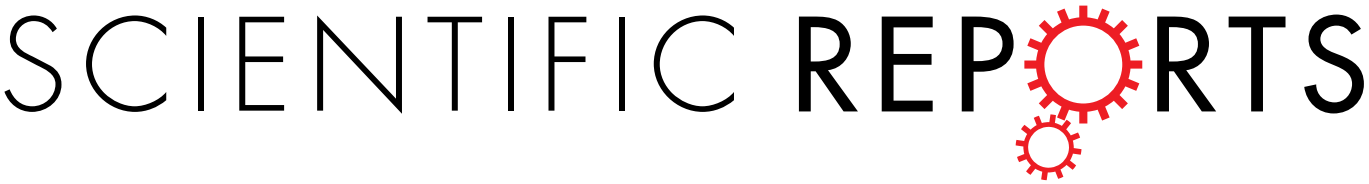

OPEN

Parity-time symmetry in coherent asymmetric double quantum wells

Si-Cong Tian[1], Ren-Gang Wan[2], Li-Jie Wang[1], Shi-Li Shu[1], Huan-Yu Lu[1,4], Xin Zhang[1,4], Cun-Zhu Tong[1], Min Xiao[3] & Li-Jun Wang[1]

Received: 3 September 2018
Accepted: 9 January 2019
Published online: 22 February 2019

A coherently prepared asymmetric double semiconductor quantum well (QW) is proposed to realize parity-time (*PT*) symmetry. By appropriately tuning the laser fields and the pertinent QW parameters, *PT*-symmetric optical potentials are obtained by three different methods. Such a coherent QW system is reconfigurable and controllable, and it can generate new approaches of theoretically and experimentally studying *PT*-symmetric phenomena.

The non-Hermitian parity-time (*PT*)-symmetric Hamiltonians, which were firstly proposed by Bender and Boettcher in 1998, have attracted great attention[1]. Because of the isomorphism between quantum Schrödinger equations and paraxial-wave equations[2], optical system becomes an ideal bed for experimentally studying *PT* symmetry. By balancing gain and loss, optical *PT* symmetry has been realized in different coupled structures, such as waveguides[3,4], lattices[5,6], micro-cavities[7,8], and can be used in the fields of unidirectional propagating[9,10], perfect absorbers[11,12], photon lasers[13,14], phonon lasers[15] and sensors[16]. In addition, several interesting phenomena, such as optical solitons[17], Bloch oscillations[18] and topological insulators[19] have also been investigated in optical *PT*-symmetric systems. However, most of the work, particularly in experiment, was based on solid-state materials. Once the structures are fabricated, the properties such as the threshold of the system are unable to be changed.

The susceptibility of host semiconductor quantum wells (QWs) can be controlled via electrical field[20–22], carrier density[23] and laser field[24]. The optical response of QWs is significantly enhanced when the frequency of light field is near resonance with the intersubband transition which has large dipole matrix element[25]. As a result, one can obtain a dramatic change in the complex dielectric constant[20–25]. Combined with electromagnetically induced transparency (EIT)[26,27], both the refractive index and the absorptive coefficient of QWs can be effectively manipulated via atomic coherence and quantum interference.

In this work, we propose to use a coherently prepared asymmetric double semiconductor QWs to obtain *PT* symmetry. Such QW systems have been proved to have the possibility to realize quantum coherence and interference[28–30]. We demonstrate that *PT*-symmetric optical potentials, such as coupled optical waveguides, one-dimensional (1D) and two-dimensional (2D) *PT*-symmetric optical lattices can be realized by different methods. Besides, it is possible to control the *PT*-symmetric properties by tuning the laser fields and the QW parameters. The realization of *PT* symmetry in coherent QW systems by laser fields have several advantages. Firstly, compared with solid-state materials with micro-structures or nano-structures, *PT*-symmetric properties in this system can be established by different methods, and can be effectively controlled by various parameters. Secondly, *PT* symmetry has been constructed theoretically[31–34] and experimentally[35] in different atomic systems. Compared with these atomic systems, semiconductor QW systems have designable and flexible of energy levels, and they are easy to be integrated and stable for practical application. Thirdly, in such systems large nonlinearity can be realized assisted by EIT[36–38], which makes it possible to observe traveling effects of lights in non-Hermitian nonlinear optical systems[39–41].

Models and Equations

We consider asymmetric double semiconductor QWs[42], which consist of a 51-monolayer (145 Å)-thick wide well (WW) and 35-monolayer (100 Å)-thick narrow well (NW). Between them there is a thickness of a 9-monolayer (25-Å)-thick $Al_{0.2}Ga_{0.8}As$ barrier, as shown in Fig. 1(a). There are ten pairs of QWs (each pair consists of one WW, one NW, and one thick barrier), which are isolated from each other by 200-Å-wide $Al_{0.2}Ga_{0.8}As$ buffer layers. All these pairs are sandwiched between nominally undoped 3500-Å-thick $Al_{0.2}Ga_{0.8}As$ layers.

[1]State Key Laboratory of Luminescence and Applications, Changchun Institute of Optics, Fine Mechanics and Physics, Chinese Academy of Sciences, Changchun, 130033, China. [2]School of Physics and Information Technology, Shaanxi Normal University, Xi'an, 710062, China. [3]Department of Physics, University of Arkansas, Fayetteville, Arkansas, 72701, USA. [4]University of Chinese Academy of Sciences, Beijing, 100049, China. Correspondence and requests for materials should be addressed to C.-Z.T. (email: tongcz@ciomp.ac.cn)

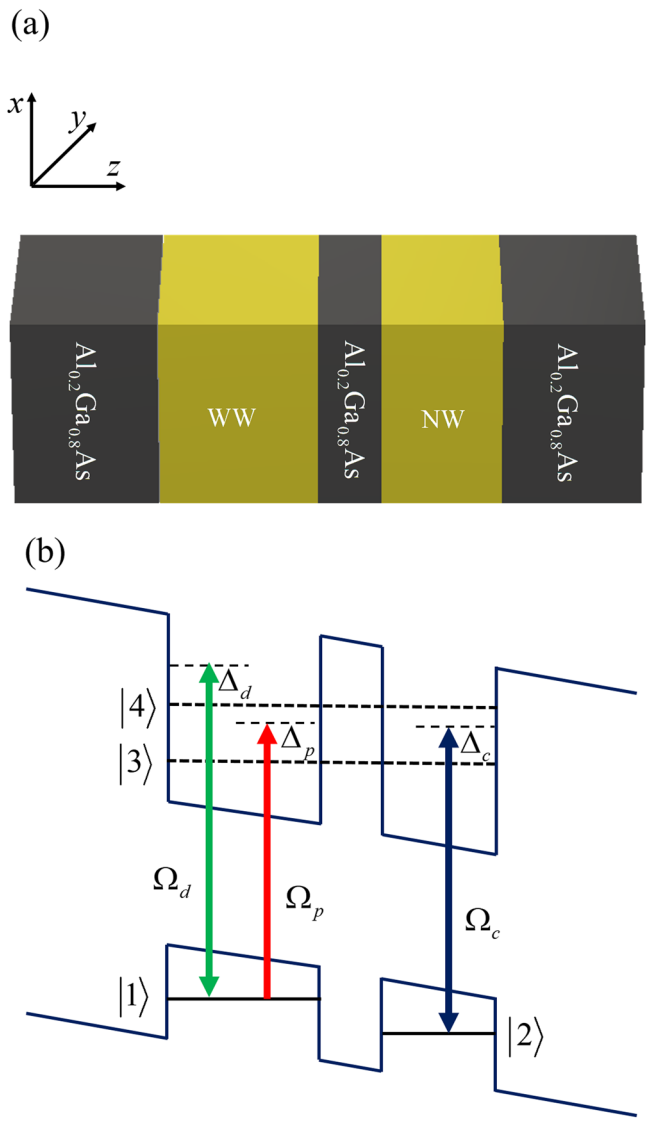

Figure 1. (**a**) Schematic of one pair of asymmetric double QWs with buffer layers. (**b**) Band diagram of the asymmetric double QWs, and z represent the wafer-growth direction.

Such asymmetric double semiconductor QWs can be treated as a four-level N configuration[28–30], as shown in Fig. 1(b). Here, levels $|1\rangle$ and $|2\rangle$ are localized hole states in a valence band, while levels $|3\rangle$ and $|4\rangle$ are delocalized bonding and antibonding states in a conduction band, arising from the tunneling effect between the WW and NW via the thin barrier, respectively. The probe field E_p with frequency ω_p probes the transition $|1\rangle \leftrightarrow |3\rangle$, while the coupling field E_c with frequency ω_c and the pump field E_d with frequency ω_d act on transitions $|2\rangle \leftrightarrow |3\rangle$ and $|1\rangle \leftrightarrow |4\rangle$ respectively. The Rabi frequency of the probe, coupling, and pump fields are $\Omega_p = \mu_{13}E_p/2\mathrm{h}$, $\Omega_c = \mu_{23}E_c/2\mathrm{h}$, and $\Omega_d = \mu_{14}E_d/2\mathrm{h}$, respectively, where μ_{ij} is the associated dipole transition matrix element, and the detuning of the probe, coupling, and pump fields are $\Delta_p = \omega_p - \omega_{31}$, $\Delta_c = \omega_c - \omega_{32}$, and $\Delta_d = \omega_d - \omega_{42}$, respectively, where ω_{ij} is the transition frequency between levels $|i\rangle$ and $|j\rangle$.

Under the condition of low QW carrier intensity, many-body effects are attributed to electron–electron interactions can be neglected[43]. In the interaction picture and under the rotating wave approximation, the Hamiltonian of the QW system can be written as ($\mathrm{h} = 1$)

$$\begin{aligned} H &= (\Delta_c - \Delta_p)|2\rangle\langle 2| - \Delta_p|3\rangle\langle 3| - \Delta_d|4\rangle\langle 4| \\ &\quad + \left[\Omega_p|1\rangle\langle 3| + \Omega_c|2\rangle\langle 3| + \Omega_d|1\rangle\langle 4| + \mathrm{H.c.}\right]. \end{aligned} \tag{1}$$

Here, H.c. is the Hamiltonian complex conjugate.

The equation of motion for the density matrix of the system under the relaxation process is

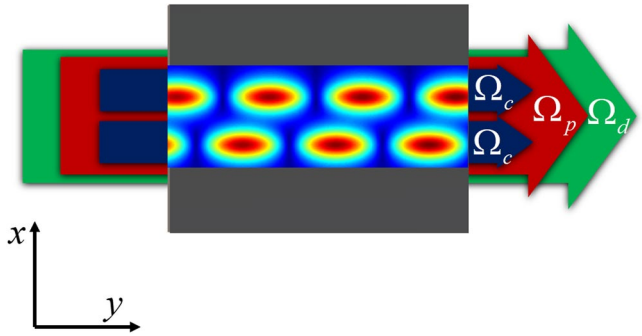

Figure 2. Schematic diagram of QW system for realizing *PT*-symmetric optical waveguides. *x* and *y* represent the transverse and longitudinal directions of laser beams.

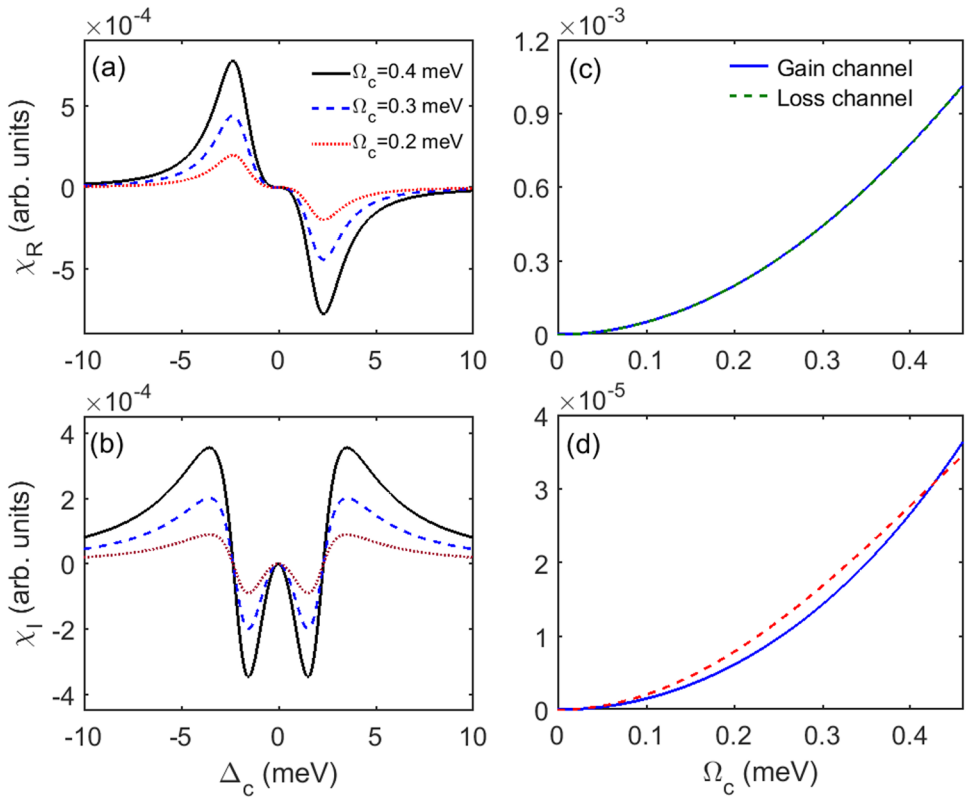

Figure 3. (**a**) Real part χ_R and (**b**) imaginary part χ_I of the susceptibility as a function of coupling detuning Δ_c for different coupling Rabi frequency, $\Omega_c = 0.4$ meV (black solid line), $\Omega_c = 0.3$ meV (blue dashed line), and $\Omega_c = 0.2$ meV (red dotted line). (**c**) Real part χ_R and (**d**) imaginary part χ_I of the susceptibility as a function of coupling Rabi frequency Ω_c for different coupling detuning, $\Delta_c = -2.278$ meV (blue solid line) and $\Delta_c = -2.360$ meV (red dashed line). The other parameters are $\Gamma_3^{dph} = \Gamma_4^{dph} = 2.58$meV, $\Gamma_{3l} = \Gamma_{4l} = 2.07$ meV, $\Gamma_{31} = \Gamma_{32} = \Gamma_{41} = \Gamma_{42} = \Gamma = 2.325$ meV, $\Omega_p = 0.01\Gamma$, $\Omega_d = 2\Gamma$, $\Delta_p = \Delta_d = 0$.

$$\dot{\rho} = -i[H, \rho] - \frac{1}{2}\{\gamma, \rho\}, \tag{2}$$

where γ is the dissipation matrix. Substituting Eq. (1) into Eq. (2), the density matrix for each element can be obtained:

$$\dot{\rho}_{22} = i\Omega_c(\rho_{32} - \rho_{23}) + \Gamma_{42}\rho_{44} + \Gamma_{32}\rho_{33} - \Gamma_2\rho_{22}, \tag{3a}$$

$$\dot{\rho}_{33} = i\Omega_c(\rho_{23} - \rho_{32}) + i\Omega_p(\rho_{13} - \rho_{31}) - \Gamma_3\rho_{33} + \Gamma_{43}\rho_{44}, \tag{3b}$$

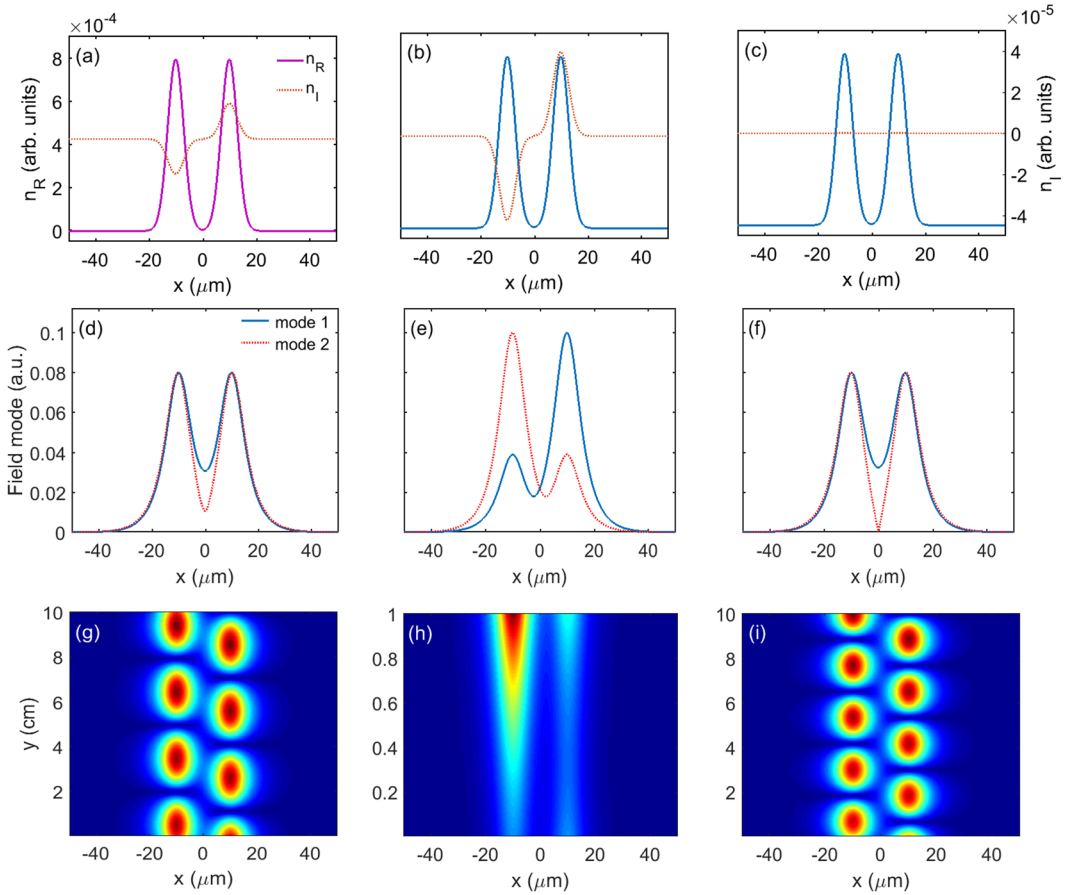

Figure 4. Real part n_R and imaginary part n_I of the refractive index as a function of position x for different cases, (**a**) $\Delta_c = -2.350$ meV (loss waveguide) and $\Delta_c = -2.300$ meV (gain waveguide), representing the condition of below threshold, (**b**) $\Delta_c = -2.386$ meV (loss waveguide) and $\Delta_c = -2.266$ meV (gain waveguide), representing the condition of above threshold, (**c**) $\Delta_c = -2.325$ meV (both waveguides), representing the condition of non-*PT* symmetry, respectively. (**d**–**f**) are filed mode of the probe laser beam according to (**a**–**c**). (**g**–**i**) are propagation properties of the probe laser beam according to (**a**–**c**). The other parameters are the same as in Fig. 3.

$$\dot{\rho}_{44} = i\Omega_d(\rho_{14} - \rho_{41}) - \Gamma_4\rho_{44}, \tag{3c}$$

$$\dot{\rho}_{12} = -i\Omega_c\rho_{13} + i\Omega_p\rho_{32} + i\Omega_d\rho_{42} - \tilde{\gamma}_{12}\rho_{12}, \tag{3d}$$

$$\dot{\rho}_{13} = -i\Omega_c\rho_{12} + i\Omega_d\rho_{43} + i\Omega_p(\rho_{33} - \rho_{11}) - \tilde{\gamma}_{13}\rho_{13}, \tag{3e}$$

$$\dot{\rho}_{14} = i\Omega_p\rho_{34} + i\Omega_d(\rho_{44} - \rho_{11}) - \tilde{\gamma}_{14}\rho_{14}, \tag{3f}$$

$$\dot{\rho}_{23} = -i\Omega_p\rho_{21} + i\Omega_c(\rho_{33} - \rho_{22}) - \tilde{\gamma}_{23}\rho_{23}, \tag{3g}$$

$$\dot{\rho}_{24} = -i\Omega_d\rho_{21} + i\Omega_c\rho_{34} - \tilde{\gamma}_{24}\rho_{24}, \tag{3h}$$

$$\dot{\rho}_{34} = i\Omega_p\rho_{14} - i\Omega_d\rho_{31} + i\Omega_c\rho_{24} - \tilde{\gamma}_{34}\rho_{34}, \tag{3i}$$

Here $\rho_{11} + \rho_{22} + \rho_{33} + \rho_{44} = 1$ and $\rho_{ij} = \rho_{ji}^*$. Γ_{ij} is the natural decay rate between levels $|i\rangle$ and $|j\rangle$. We assume that the decay rates from levels $|3\rangle$ and $|4\rangle$ in the conduction band to levels $|1\rangle$ and $|2\rangle$ in the valence band are identical, there are, $\Gamma_{31} = \Gamma_{32}$ and $\Gamma_{41} = \Gamma_{42}$. There is also no decay in the valence band or conduction band, so we conclude that $\Gamma_{21} = \Gamma_{43} = 0$. $\Gamma_i = \sum_j^{i-1}\Gamma_{ij}$ denotes the total decay rate of level $|i\rangle$. We define $\tilde{\gamma}_{12} = \gamma_{12} + i(\Delta_p - \Delta_c)$, $\tilde{\gamma}_{13} = \gamma_{13} + i\Delta_p$, $\tilde{\gamma}_{14} = \gamma_{14} + i\Delta_d$, $\tilde{\gamma}_{23} = \gamma_{23} + i\Delta_c$, $\tilde{\gamma}_{24} = \gamma_{24} + i(\Delta_c + \Delta_d - \Delta_p)$, and $\tilde{\gamma}_{34} = \gamma_{34} + i(\Delta_d - \Delta_p)$, where $\gamma_{ij} = (\Gamma_i + \Gamma_j)/2$.

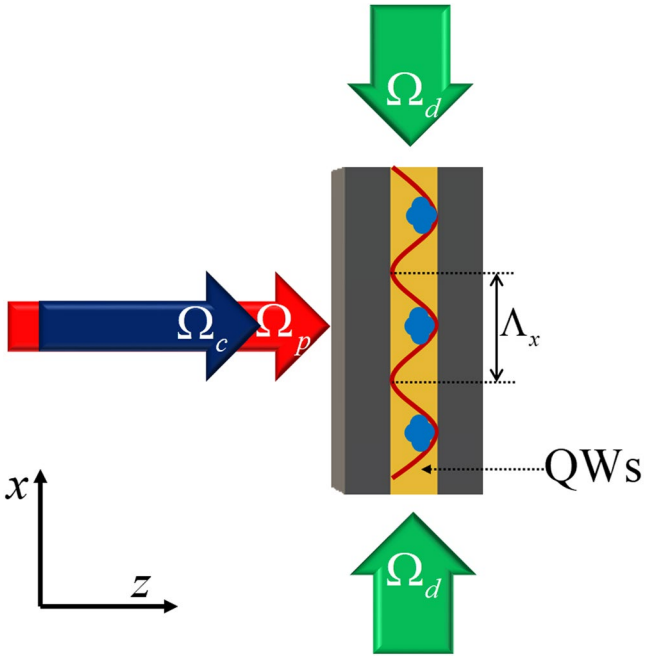

Figure 5. Schematic diagram of QW system for realizing *PT*-symmetric optical lattices. Electron density of QW is modulated in *x* direction.

In such QW systems, $\Gamma_3 = \Gamma_{3l} + \Gamma_3^{dph}$ and $\Gamma_4 = \Gamma_{4l} + \Gamma_4^{dph}$, where Γ_{3l} and Γ_{4l} are the population decay rates of subbands $|3\rangle$ and $|4\rangle$ respectively, resulting from longitudinal-optical phonon emission events at low temperature, and Γ_3^{dph} and Γ_4^{dph} are the dephasing decay rates of quantum coherence due to electron–electron scattering, phonon scattering processes; and elastic interface roughness. Based on the previous studies, we assume that Γ_{3l} can be equal to Γ_{4l}, and Γ_3^{dph} can be equal to Γ_4^{dph}. Therefore, $\Gamma_{31} = \Gamma_{32} = \Gamma_{41} = \Gamma_{42} = \Gamma$ can be presented. In addition, we assume there is no interference or dephasing between levels $|3\rangle$ and $|4\rangle$, which can be realized based on the appropriate reduction of the temperature[44].

The susceptibility of the QW medium can be obtained through the expression $\chi = N\mu_{13}/\varepsilon_0 E_p \cdot \rho_{31} = N\mu_{13}^2/2\varepsilon_0 \hbar\Omega_p \cdot \rho_{31}$, where N is the electron density of the QWs, and ρ_{31} can be obtained by Eq. (3). $\chi = \chi_R + i\chi_I$, where χ_R describes the dispersion properties of the probe field, while χ_I describes the absorption properties of the probe field with $\chi_I > 0$ ($\chi_I < 0$) indicating loss (gain).

The refractive index of the QW medium can be written as $n = \sqrt{\varepsilon_c + \chi}$. Here $\varepsilon_c = n_c^2$ corresponding to the complex dielectric constant of the host QW medium, and n_c is its refractive index when light is far detuned from the resonance. χ denotes the change in the susceptibility[22,23], which results from the coherent contract via the coupling and pump fields near the resonance. Generally, $\chi = \varepsilon_c$, then we have $n \approx \sqrt{\varepsilon_c} + \chi/2\sqrt{\varepsilon_c} = n_c + \chi/2n_c = n_c + \chi_R/2n_c + i\chi_I/2n_c$. We define the real and imaginary parts of the refractive index as n_R and n_I, with n_c being the background index of the system. Thus, $n = n_c + n_R + in_I$, where $n_R = \chi_R/2n_0$ and $n_I = \chi_I/2n_0$. To achieve *PT* symmetry, the condition of $n_R(r) = n_R(-r)$ and $n_I(r) = -n_I(-r)$ must be satisfied. And for simplicity, we use the unit $N\mu_{13}^2/4\varepsilon_0 \hbar n_0$ in the following calculations.

Results

***PT*-symmetric optical waveguides.** In order to realize *PT*-symmetric optical waveguides, we use a pair of coupling laser beams to form two coupled waveguides. Such pair of beams propagate in QWs along *y* direction. Then, a pump and a probe laser beams with wider laser dimension propagate in the same direction as those of the coupling beams. The schematic diagram is shown in Fig. 2. The pair of coupling laser beams have an identical Gaussian intensity profile so that the total spatial intensity distribution of them varying in *x* direction is

$$I_c(x) = Ae^{\frac{-(x-a)^2}{2\sigma^2}} + Ae^{\frac{-(x+a)^2}{2\sigma^2}}, \tag{4}$$

where A and a are the constant and the half separation between the two waveguides respectively. $2\sqrt{2\ln 2}\,\sigma$ can describe the full width at half maximum (FWHM) of the waveguides. By choosing two different detuning of the coupling fields, gain can be introduced to one waveguide and loss can be introduced to the other, even though other parameters are identical. In such consideration, the refractive index in each waveguide spatially varies only with the intensity of the coupling.

To realize gain and absorption in two waveguides simultaneously, different detuning of the coupling fields need to be found. For sake of it, we calculate the real (dispersion) χ_R and imaginary (gain or absorption) χ_I parts of the susceptibility as a function of Δ_c, and show the results in Fig. 3(a,b), respectively. The intensity of the

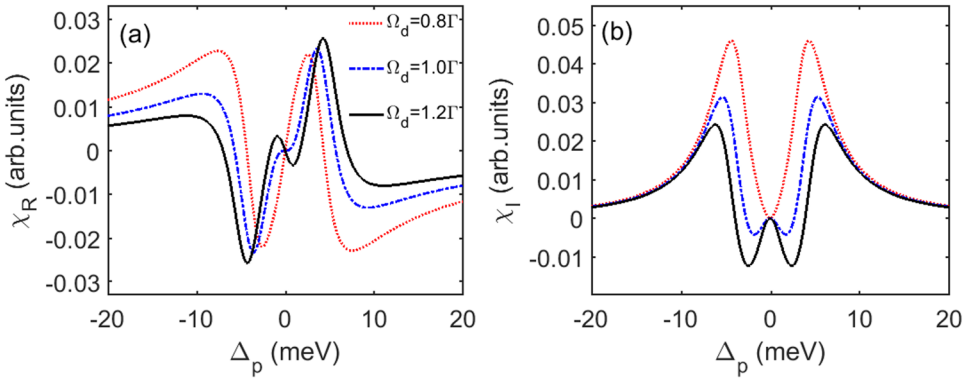

Figure 6. (**a**) Real part χ_R and (**b**) imaginary part χ_I of the susceptibility as a function of probe detuning Δ_p for different pump Rabi frequency, $\Omega_d = 0.8\Gamma$ (red dotted line), $\Omega_d = \Gamma$ (blue dashed line), and $\Omega_d = 1.2\Gamma$ (black solid line). The parameters are $\Omega_c = \Gamma$ and $\Delta_c = \Delta_d = 0$. The other parameters are the same as in Fig. 3.

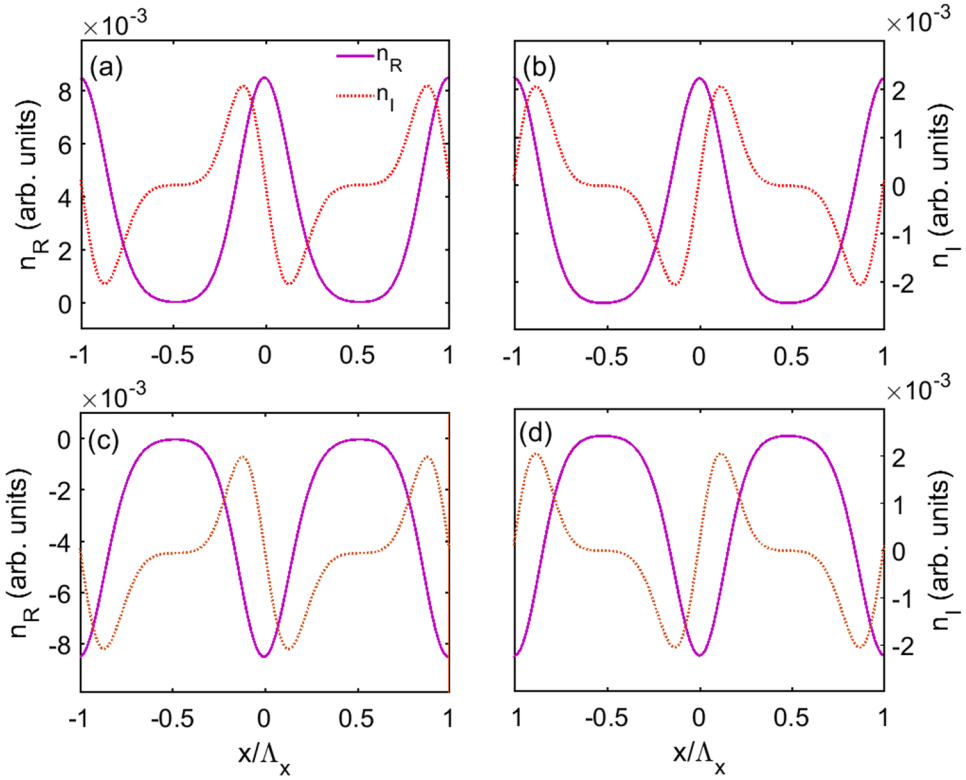

Figure 7. Real part n_R and imaginary part n_I of the refractive index as a function of position x for unchanged absolute value and different signs of Δ_p and $\delta\Omega_d$, respectively, (**a**) $\Delta_p = 2.592$ meV and $\delta\Omega_d = 0.1\Gamma$, (**b**) $\Delta_p = 2.592$ meV and $\delta\Omega_d = -0.1\Gamma$, (**c**) $\Delta_p = -2.592$ meV and $\delta\Omega_d = 0.1\Gamma$, (**d**) $\Delta_p = -2.592$ meV and $\delta\Omega_d = -0.1\Gamma$. The parameters are $\Omega_{d0} = \Gamma$. The other parameters are the same as in Fig. 6.

coupling field in each waveguide is corresponding to Gaussian profile, so χ_I needs to get larger with increasing coupling intensity. For this reason, we only consider a negative value of the coupling detuning. It can be seen from the figures that for different value of Ω_c, χ_R reaches to the maximum value, and χ_I is close to zero at $\Delta_c = -2.325\Gamma$. At the vicinity of the zero point, gain is obtained on the left side, and absorption is abstained on the right side. This property called refractive index enhancement with vanishing absorption, has been demonstrated in the early papers[45–49].

In order to realize gain and loss in two waveguides simultaneously by using two different coupling detuning and maintain other parameters identical, the relation between the susceptibility and the coupling intensity needs to be established. Therefore, we choose $\Delta_c = -2.360\Gamma$ and $\Delta_c = -2.278\Gamma$ in two waveguides, and draw χ_R and χ_I as a function of Ω_c shown in Fig. 3(c,d). It can be seen that with selected coupling detuning, the curves of χ_R are identical, and the curves of χ_I are matched with slight difference, respectively. It should be noted that, in

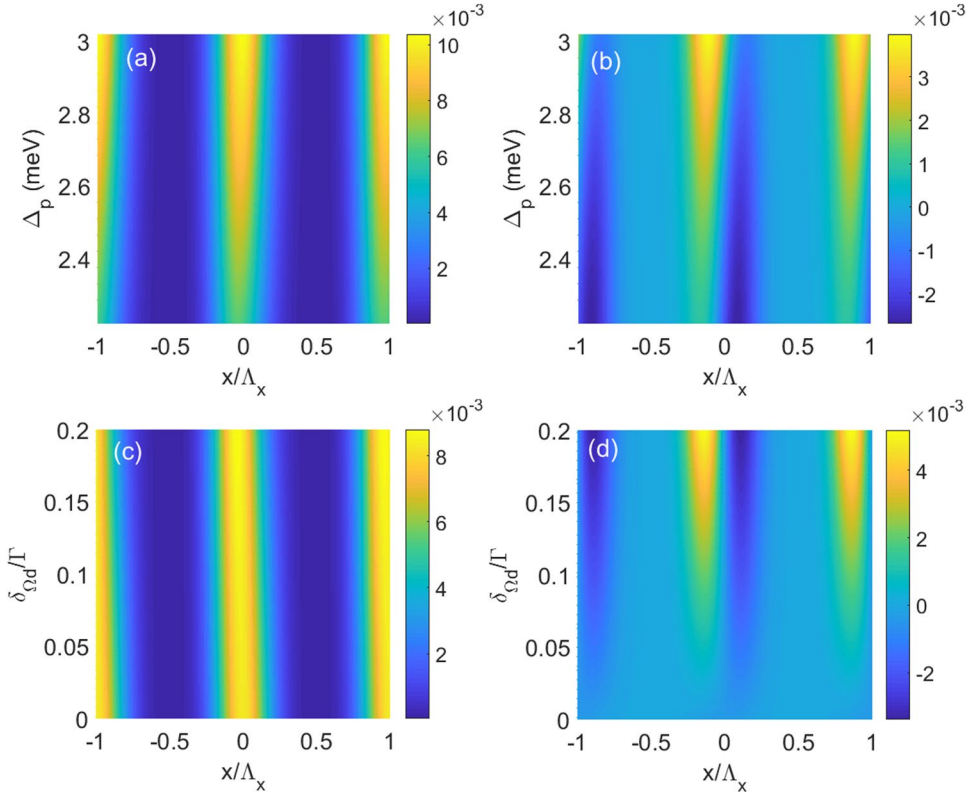

Figure 8. (**a**) Real part n_R and (**b**) imaginary part n_I of the refractive index as functions of position x and probe detuning Δ_p. The parameters are $\delta\Omega_d = 0.1\Gamma$. (**c**) Real part n_R and (**d**) imaginary part n_I of the refractive index as functions of position x and modulation intensity $\delta\Omega_d$. The parameters are $\Delta_p = 2.592$ meV. The other parameters are the same as in Fig. 7.

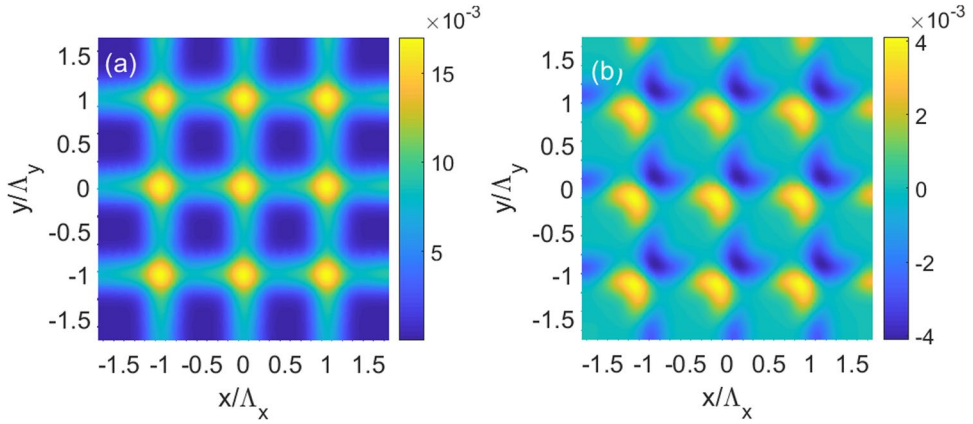

Figure 9. (**a**) Real part n_R and (**b**) imaginary part n_I of the refractive index as functions of position x and position y. The parameters are $\Delta_p = 2.592$ meV and $\delta\Omega_d = 0.1\Gamma$. The other parameters are the same as in Fig. 7.

Fig. 3(d) we flipped the curve of the gain one by multiplying a minus sign to compare the two curves of gain and loss directly.

Based on the above analysis, firstly, we demonstrate the possibility of realizing spatial modulation of the refractive index. Making use of Eq. (4), and choosing the FWHM ($2\sqrt{2\ln 2}\,\sigma$) as 7 μm and the separation between the two waveguides as 20 μm, we plot the real n_R and the imaginary n_I parts of the refractive index as a function of x shown in Fig. 4(a–c). It can be seen from the figures that the real part of the refractive index n_R is an even function of x, while that of imaginary part n_I is an odd function of x. By changing the electron intensity of QW, The absolute values of n_R and n_I can be modified with equal scale simultaneously with the changes of the electron intensity of QW.

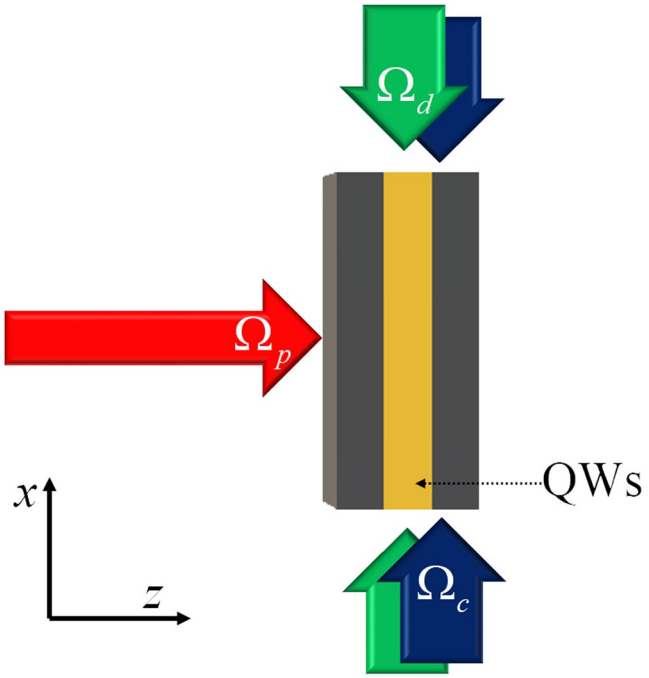

Figure 10. Schematic diagram of QW system for realizing *PT*-symmetric optical lattices.

By controlling the ratio of the real and imaginary parts of the refractive index, we can adjust the condition of the system below or above the *PT*-symmetric threshold. It can be seen from Fig. 3(a,b) that χ_R changes less than χ_I at the vicinity of zero point ($\Delta_c = -2.325\Gamma$). Therefore, we can alter the coupling detuning in the waveguides to control the ratio. For instance, with different values of the coupling detuning, the ratio of the real and imaginary parts is 12 and 80, and the system can be operated below (Fig. 4(a)) or above (Fig. 4(b)) the *PT*-symmetric threshold respectively. In addition, when the coupling detuning used in both waveguides is -2.325Γ, the system even becomes a non-symmetric one with much larger ratio (Fig. 4(c)).

Secondly, we present the field modes in the waveguides in Fig. 4(d–f) corresponding to Fig. 4(a–c), respectively. When the condition of the system is below the threshold (Fig. 4(a)), the *PT* symmetry condition is satisfied, the eigenvalues should be real, and the field modes should be symmetric. However, because of the imperfect *PT* symmetry condition, the eigenvalues have a very small imaginary part, and the two field modes are slightly asymmetric, as shown in Fig. 4(d). For the case of above the threshold (Fig. 4(b)), that is, the *PT* symmetry is broken, the eigenvalues become complex, where the imaginary part of the refractive index represents the gain or loss for each filed mode. Figure 4(e) illustrates that, the light modes become strongly asymmetric. For the non-symmetric one (Fig. 4(c)), the light modes are perfectly symmetric, which is shown in Fig. 4(f).

Thirdly, we show in Fig. 4(g–i) the propagation characteristics of the probe beam according to the condition of Fig. 4(a–c) respectively. When the condition of the system is below threshold, the probe beam oscillates periodically between the two waveguides, as show in Fig. 4(g). When the case is above the threshold, it can be seen from Fig. 4(h) that an exponentially growing mode occurs, which signifies the onset of *PT* symmetry breaking. For the passive waveguides, the probe beam also oscillates periodically (Fig. 4(i)), which is similar to the case of below threshold. However, the oscillation period in Fig. 4(i) is shorter than that of in Fig. 4(g).

In a practical system, it is very difficult to realize perfect *PT*-symmetric condition. So, we evaluate the degrees of asymmetry of the system by analyzing the asymmetry function of $\Delta(x) = n(x) - n^*(-x)$, and find that the degree of asymmetry is very small. Therefore, it is manageable and has little impact on practical experiments.

***PT*-symmetric optical lattices—Type I.** In this part, we first consider an 1D optical lattices of period Λ_x along x direction, and in each lattices the electron density of QWs is spatially modulated. The electron density in the ith trap can exhibit a Gaussian distribution $N_i(x, y) = Ne^{-(x-x_i)^2/\sigma_x^2}$, where N is the electron density of a homogeneous QW sample, x_i is the ith trap center, and σ_x is the half width. The modulation of electron density of QWs can be achieved by using high order surface grating[50,51]. We further consider a pump laser field with periodically modulated intensity $\Omega_d = \Omega_{d0} + \delta\Omega_d \sin[2\pi(x - x_i)/\Lambda_x]$, which can be easily achieved in experiment by using an imperfect standing-wave (SW) field with unequal forward and backward components. We show the schematic diagram of QW system in Fig. 5. The probe field and coupling filed propagate along z direction, and the SW pump fields propagate along x direction.

First, we calculate the real χ_R and imaginary χ_I parts of the susceptibility as a function of Δ_p for varying value of Ω_d by solving Eq. (3) without modulation of pump intensity or the electron density, and the corresponding results are shown in Fig. 6. It can be seen from red dotted line in Fig. 6(b) that when $\Omega_d = 0.8\Gamma$, a typical EIT with positive value (loss) is realized. With increasing value of Ω_d, at both sides of the EIT windows, χ_I becomes positive (gain), which is knew as coherent Raman gain without population inversion [blue dashed line and black

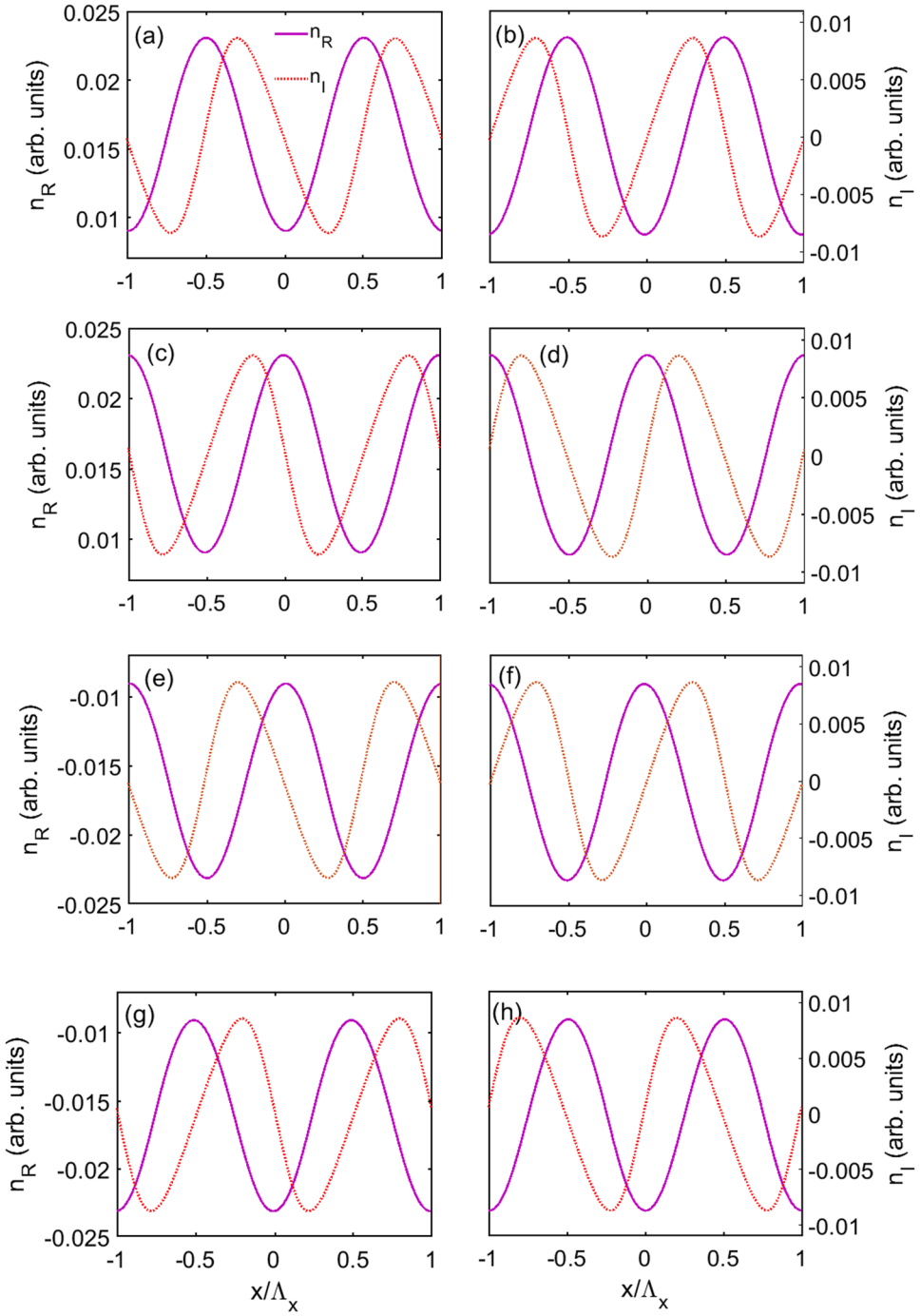

Figure 11. Real part n_R and imaginary part n_I of the refractive index as a function of position x for unchanged absolute value and different signs of Δ_p, $\delta\Omega_c$ and $\delta\Omega_d$, respectively, (**a**) $\Delta_p = 2.525$ meV, $\delta\Omega_c = 0.3\Gamma$ and $\delta\Omega_d = 0.1\Gamma$, (**b**) $\Delta_p = 2.525$ meV, $\delta\Omega_c = 0.3\Gamma$ and $\delta\Omega_d = -0.1\Gamma$, (**c**) $\Delta_p = 2.525$ meV, $\delta\Omega_c = -0.3\Gamma$ and $\delta\Omega_d = 0.1\Gamma$, (**d**) $\Delta_p = 2.525$ meV, $\delta\Omega_c = -0.3\Gamma$ and $\delta\Omega_d = -0.1\Gamma$, (**e**) $\Delta_p = -2.525$ meV, $\delta\Omega_c = 0.3\Gamma$ and $\delta\Omega_d = 0.1\Gamma$, (**f**) $\Delta_p = -2.525$ meV, $\delta\Omega_c = 0.3\Gamma$ and $\delta\Omega_d = -0.1\Gamma$, (**g**) $\Delta_p = -2.525$ meV, $\delta\Omega_c = -0.3\Gamma$ and $\delta\Omega_d = 0.1\Gamma$, (**h**) $\Delta_p = -2.525$ meV, $\delta\Omega_c = -0.3\Gamma$ and $\delta\Omega_d = -0.1\Gamma$. The parameters are $\Omega_{c0} = 3\Gamma$ and $\Omega_{d0} = \Gamma$. The other parameters are the same as in Fig. 6.

solid line in Fig. 6(b)]. Meanwhile, χ_R changes form positive dispersion to negative dispersion in the vicinity of EIT window, as shown in Fig. 6(a). The figures indicate that it is possible to realize *PT* symmetry by choosing suitable modulations.

Then, with modulation of the pump intensity and electron density, we calculate the real (n_R) and imaginary parts (n_I) of the refractive index as a function of x and show the results in Fig. 7. Figure 7(a) shows the condition of $\Delta_p = 2.592$ meV and $\delta\Omega_d = 0.1\Gamma$. The value of Δ_p is chosen according to blue dashed line in Fig. 6(b), where χ_I has zero value around $\Delta_p = 2.592$ meV, and thus it exhibits gain or absorption if Δ_p is slightly tuned away from

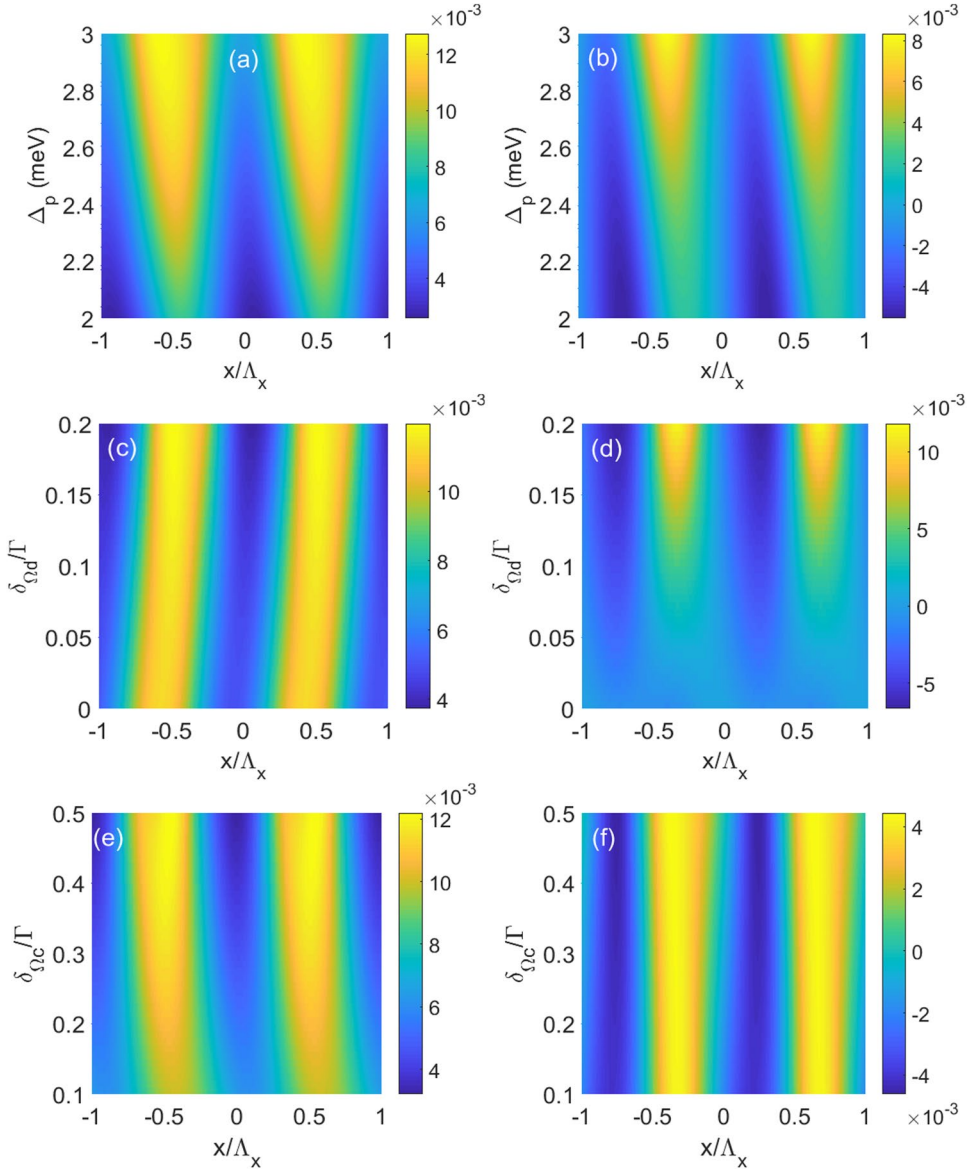

Figure 12. (**a**) Real part n_R and (**b**) imaginary part n_I of the refractive index as functions of position x and probe detuning Δ_p. The parameters are $\delta\Omega_c = 0.3\Gamma$ and $\delta\Omega_d = 0.1\Gamma$. (**c**) Real part n_R and (**d**) imaginary part n_I of the refractive index as functions of position x and modulation intensity $\delta\Omega_d$. The parameters are $\Delta_p = 2.525$ meV and $\delta\Omega_c = 0.3\Gamma$. (**e**) Real part n_R and (**f**) imaginary part n_I of the refractive index as functions of position x and modulation intensity $\delta\Omega_c$. The parameters are $\Delta_p = 2.525$ meV and $\delta\Omega_d = 0.1\Gamma$. The other parameters are the same as in Fig. 11.

this point. It can be seen that n_R is an even function of the lattice position x, while n_I is an odd function of lattice position x with balance gain and loss. Such results clearly indicate that PT symmetry is built in QW system by modulating the pump field and the electron density.

In Figs 7(b) and 6(d), we further show the cases for the same absolute value of Δ_p and $\delta\Omega_d$ as that of in Fig. 7(a), but with different sign of them. The results show that the PT-symmetric properties are maintained in all cases. However, the relation between n_R and n_I are different. It is found that positive (negative) value of Δ_p results in the positive (negative) value of n_R and have no effect on the profile of n_I. On the other hand, the sign of $\delta\Omega_d$ determines the position of gain and loss in each period, for instance, with positive (negative) value of $\delta\Omega_d$, n_I is gain (loss) in one half period $-0.5 \leq x/\Lambda_x \leq 0$. The understanding of impacts of the parameters on spatial features of the refractive index is important because of its potential application, such as asymmetric light diffraction[52,53].

We next check what will happen if the absolute value of Δ_p and $\delta\Omega_d$ is changed. To do so, we plot 2D n_R and n_I as functions of x and Δ_p in Fig. 8(a,b), and as functions of x and $\delta\Omega_d$ in Fig. 8(c,d), respectively. The figures clearly show that n_R and n_I are modulated along x direction for varying Δ_p or $\delta\Omega_d$. In addition, the profile of n_I is much more sensitive to the parameters than that of n_R. When Δ_p or $\delta\Omega_d$ is detuned from the value used in Fig. 7(a), through n_R is maintained an even property, n_I losses odd property, where the loss in one half period is not equal to

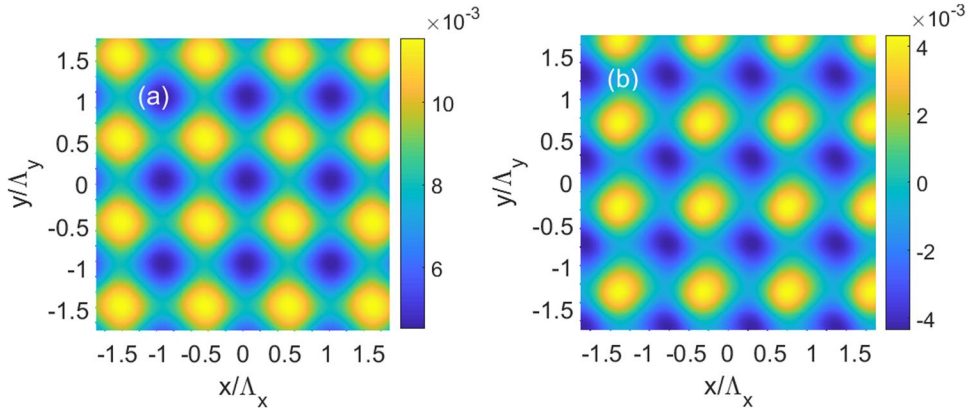

Figure 13. (**a**) Real part n_R and (**b**) imaginary part n_I of the refractive index as functions of position x and position y. The parameters are $\Delta_p = 2.525$ meV, $\delta\Omega_c = 0.3\Gamma$ and $\delta\Omega_d = 0.1\Gamma$. The other parameters are the same as in Fig. 11.

the gain in the other half. Therefore, *PT* symmetry is destroyed in QW system because of the nonlinear response of n_I to Δ_p or $\delta\Omega_d$.

Last, our goal is to realize 2D modulation of refractive index as functions of x and y, and this can be achieved by 2D modulation of the electron density and pump field, which are

$$N_i(x, y) = Ne^{-(x-x_i)^2/\sigma_x^2-(y-y_i)^2/\sigma_y^2}, \tag{5a}$$

$$\Omega_d = \Omega_{d0} + 0.5\ \delta\Omega_d\{\sin[2\pi(x - x_i)/\Lambda_x] + \sin[2\pi(y - y_i)/\Lambda_y]\}, \tag{5b}$$

We plot in Fig. 9(a,b) the top view of n_R and n_I as functions of x and y using the same parameters in Fig. 7(a), respectively. The results clearly show that n_R is an even functions of x and y, while n_I is an odd functions of x and y, therefore, 2D *PT*-symmetric optical lattices is realized in QW systems.

***PT*-symmetric optical lattices—Type II.** In this part, we show that *PT* symmetry can also be achieved by modulating both pump and coupling fields. The schematic diagram of the system is shown in Fig. 10, where the probe field propagates along z direction, and the SW coupling and SW pump fields propagate along x direction. Therefore, we have modulated coupling and pump fields, $\Omega_c = \Omega_{c0} + \delta\Omega_c\cos[2\pi(x - x_i)/\Lambda_x]$, $\Omega_d = \Omega_{d0} + \delta\Omega_d\sin[2\pi(x - x_i)/\Lambda_x]$.

First, we plot the real and imaginary parts of the refractive index (n_R and n_I) as a function of x in Fig. 11 for different cases. Figure 11(a) shows the condition of $\Delta_p = 2.592$ meV and the modulation intensities $\delta\Omega_c = 0.3\Gamma$ and $\delta\Omega_d = 0.1\Gamma$. It can be seen from figure that the *PT* symmetry is appears, where n_R is an even function of x, and n_I is an odd function of x. The relations of n_R and n_I can also be modified by changing the sign of the detuning Δ_p and the modulation intensities $\delta\Omega_c$ and $\delta\Omega_d$, and the changing of their sign will not destroy the *PT* symmetry. There are eight kinds of combinations of these three parameters, corresponding to eight kinds of spatial refractive index, and we plot the other seven kinds in Fig. 11(b–h). It can be found that Δ_p, $\delta\Omega_c$ or $\delta\Omega_d$ have different impacts on the features of n_R and n_I. More specifically, Δ_p determines n_R being positive or negative, and $\delta\Omega_c$ determines the monotonicity of n_R, and $\delta\Omega_d$ determines the positions of the gain and loss in one period.

We also check the impact of absolute value of Δ_p, $\delta\Omega_c$ or $\delta\Omega_d$ on the properties of *PT*-symmetric system. Therefore, we plot 2D n_R and n_I as functions of x and Δ_p in Fig. 12(a,b), as functions of x and $\delta\Omega_d$ in Fig. 12(c,d), and as functions of x and $\delta\Omega_c$ in Fig. 12(e,f), respectively. The figures clearly show that n_R and n_I are modulated along x direction for varying Δ_p, $\delta\Omega_c$ or $\delta\Omega_d$. However, when these parameters are detuned form the value used in Fig. 11(a), the system will loss the *PT*-symmetric properties.

Last, we show that it is possible to realize 2D *PT*-symmetric optical lattices by applying 2D modulation of the pump and coupling laser fields, which are

$$\Omega_c = \Omega_{c0} + 0.5\ \delta\Omega_c\{\cos[2\pi(x - x_i)/\Lambda_x] + \cos[2\pi(y - y_i)/\Lambda_y]\}, \tag{6a}$$

$$\Omega_d = \Omega_{d0} + 0.5\ \delta\Omega_d\{\sin[2\pi(x - x_i)/\Lambda_x] + \sin[2\pi(y - y_i)/\Lambda_y]\}, \tag{6b}$$

Using the same parameters in Fig. 11(a), we calculate n_R and n_I as functions of x and y, and show the tope view of n_R and n_I as functions of x and $y$in Fig. 13(a,b), respectively. The results indicate that 2D *PT*-symmetric optical lattices can be achieved, with n_R being an even functions of x and y, and n_I being an odd functions of x and y, respectively.

Conclusion

In conclusion, we have demonstrated that coherent asymmetric double semiconductor QWs can be an ideal candidate for studying *PT* symmetry. We have showed that *PT*-symmetric optical waveguides can be realized by using two coupling fields with different detuning, 1D and 2D *PT*-symmetric optical lattices can be realized by spatial modulation of pump laser fields and the electron density of QWs, or by spatial modulation of pump and coupling fields. In addition, the *PT*-symmetric properties realized in QW systems, such as the relation between the real and the imaginary parts of the complex refractive indices, can be controlled by changing the laser fields and the parameters of QWs.

References

1. Bender, C. M. & Boettcher, S. Real spectra in non-Hermitian Hamiltonians having PT symmetry. *Physical Review Letters* **80**, 5243–5246 (1998).
2. El-Ganainy, R., Makris, K. G., Christodoulides, D. N. & Musslimani, Z. H. Theory of coupled optical PT-symmetric structures. *Opt. Lett.* **32**, 2632–2634 (2007).
3. Ruter, C. E. *et al*. Observation of parity-time symmetry in optics. *Nat Phys* **6**, 192–195 (2010).
4. Guo, A. *et al*. Observation of PT-Symmetry Breaking in Complex Optical Potentials. *Physical Review Letters* **103**, 093902 (2009).
5. Regensburger, A. *et al*. Parity-time synthetic photonic lattices. *Nature* **488**, 167–171 (2012).
6. Wimmer, M. *et al*. Observation of optical solitons in PT-symmetric lattices. *Nature Communications* **6**, 7782 (2015).
7. Peng, B. *et al*. Parity-time-symmetric whispering-gallery microcavities. *Nat Phys* **10**, 394–398 (2014).
8. Chang, L. *et al*. Parity-time symmetry and variable optical isolation in active-passive-coupled microresonators. *Nat Photon* **8**, 524–529 (2014).
9. Feng, L. *et al*. Experimental demonstration of a unidirectional reflectionless parity-time metamaterial at optical frequencies. *Nat Mater* **12**, 108–113 (2013).
10. Lin, Z. *et al*. Unidirectional Invisibility Induced by PT-Symmetric Periodic Structures. *Physical Review Letters* **106**, 213901 (2011).
11. Longhi, S. PT-symmetric laser absorber. *Physical Review A* **82**, 031801 (2010).
12. Chong, Y. D., Ge, L., Cao, H. & Stone, A. D. Coherent Perfect Absorbers: Time-Reversed Lasers. *Physical Review Letters* **105**, 053901 (2010).
13. Hodaei, H., Miri, M.-A., Heinrich, M., Christodoulides, D. N. & Khajavikhan, M. Parity-time-symmetric microring lasers. *Science* **346**, 975–978 (2014).
14. Feng, L., Wong, Z. J., Ma, R.-M., Wang, Y. & Zhang, X. Single-mode laser by parity-time symmetry breaking. *Science* **346**, 972–975 (2014).
15. Jing, H. *et al*. PT-Symmetric Phonon Laser. *Physical Review Letters* **113**, 053604 (2014).
16. Fleury, R., Sounas, D. & Alù, A. An invisible acoustic sensor based on parity-time symmetry. *Nature Communications* **6**, 5905 (2015).
17. Musslimani, Z. H., Makris, K. G., El-Ganainy, R. & Christodoulides, D. N. Optical Solitons in PT Periodic Potentials. *Physical Review Letters* **100**, 030402 (2008).
18. Longhi, S. Bloch Oscillations in Complex Crystals with PT-Symmetry. *Physical Review Letters* **103**, 123601 (2009).
19. Liang, G. Q. & Chong, Y. D. Optical Resonator Analog of a Two-Dimensional Topological Insulator. *Physical Review Letters* **110**, 203904 (2013).
20. Fejer, M. M., Yoo, S. J. B., Byer, R. L., Harwit, A. & HarrisJr, J. S. Observation of extremely large quadratic susceptibility at 9.6–10.8 um in electric-field-biased AlGaAs quantum wells. *Physical Review Letters* **62**, 1041–1044 (1989).
21. Sirtori, C., Capasso, F., Sivco, D. L. & Cho, A. Y. Giant, triply resonant, third-order nonlinear susceptibility in coupled quantum wells. *Physical Review Letters* **68**, 1010–1013 (1992).
22. Zhang, L. Electric field effect on the linear and nonlinear intersubband refractive index changes in asymmetrical semiparabolic and symmetrical parabolic quantum wells. *Superlattices and Microstructures* **37**, 261–272 (2005).
23. Kuhn, K. J., Iyengar, G. U. & Yee, S. Free carrier induced changes in the absorption and refractive index for intersubband optical transitions in AlxGa1−xAs/GaAs/AlxGa1−xAs quantum wells. *Journal of Applied Physics* **70**, 5010–5017 (1991).
24. Frogley, M. D., Dynes, J. F., Beck, M., Faist, J. & Phillips, C. C. Gain without inversion in semiconductor nanostructures. *Nature Materials* **5**, 175 (2006).
25. West, L. C. & Eglash, S. J. First observation of an extremely large-dipole infrared transition within the conduction band of a GaAs quantum well. *Applied Physics Letters* **46**, 1156–1158 (1985).
26. Silvestri, L., Bassani, F., Czajkowski, G. & Davoudi, B. Electromagnetically induced transparency in asymmetric double quantum wells. *The European Physical Journal B - Condensed Matter and Complex Systems* **27**, 89–102 (2002).
27. Phillips, M. & Wang, H. Electromagnetically induced transparency due to intervalence band coherence in a GaAs quantum well. *Opt. Lett.* **28**, 831–833 (2003).
28. Yang, W.-X. & Lee, R.-K. Controllable entanglement and polarization phase gate in coupled double quantum-well structures. *Opt. Express* **16**, 17161–17170 (2008).
29. Zhu, C. & Huang, G. Slow-light solitons in coupled asymmetric quantum wells via interband transitions. *Physical Review B* **80**, 235408 (2009).
30. Luo, X. Q., Wang, D. L., Zhang, Z. Q., Ding, J. W. & Liu, W. M. Nonlinear optical behavior of a four-level quantum well with coupled relaxation of optical and longitudinal phonons. *Physical Review A* **84**, 033803 (2011).
31. Sheng, J., Miri, M.-A., Christodoulides, D. N. & Xiao, M. PT-symmetric optical potentials in a coherent atomic medium. *Physical Review A* **88**, 041803 (2013).
32. Li, H.-j, Dou, J.-p & Huang, G. PT symmetry via electromagnetically induced transparency. *Opt. Express* **21**, 32053–32062 (2013).
33. Hang, C., Huang, G. & Konotop, V. V. PT Symmetry with a System of Three-Level Atoms. *Physical Review Letters* **110**, 083604 (2013).
34. Wang, X. & Wu, J.-H. Optical PT-symmetry and PT-antisymmetry in coherently driven atomic lattices. *Opt. Express* **24**, 4289–4298 (2016).
35. Zhang, Z. *et al*. Observation of Parity-Time Symmetry in Optically Induced Atomic Lattices. *Physical Review Letters* **117**, 123601 (2016).
36. Kang, H. & Zhu, Y. Observation of Large Kerr Nonlinearity at Low Light Intensities. *Physical Review Letters* **91**, 093601 (2003).
37. Schmidt, H. & Imamoglu, A. Giant Kerr nonlinearities obtained by electromagnetically induced transparency. *Opt. Lett.* **21**, 1936–1938 (1996).
38. Sheng, J., Yang, X., Wu, H. & Xiao, M. Modified self-Kerr-nonlinearity in a four-level N-type atomic system. *Physical Review A* **84**, 053820 (2011).
39. Abdullaev, F. K., Kartashov, Y. V., Konotop, V. V. & Zezyulin, D. A. Solitons in PT-symmetric nonlinear lattices. *Physical Review A* **83**, 041805 (2011).
40. Hang, C., Zezyulin, D. A., Konotop, V. V. & Huang, G. Tunable nonlinear parity-time-symmetric defect modes with an atomic cell. *Opt. Lett.* **38**, 4033–4036 (2013).

41. Ramezani, H., Kottos, T., El-Ganainy, R. & Christodoulides, D. N. Unidirectional nonlinear PT-symmetric optical structures. *Physical Review A* **82**, 043803 (2010).
42. Roskos, H. G. *et al*. Coherent submillimeter-wave emission from charge oscillations in a double-well potential. *Physical Review Letters* **68**, 2216–2219 (1992).
43. Nikonov, D. E., Imamoğlu, A., Butov, L. V. & Schmidt, H. Collective Intersubband Excitations in Quantum Wells: Coulomb Interaction versus Subband Dispersion. *Physical Review Letters* **79**, 4633–4636 (1997).
44. Wu, J.-H. *et al*. Ultrafast All Optical Switching via Tunable Fano Interference. *Physical Review Letters* **95**, 057401 (2005).
45. Scully, M. O. Enhancement of the index of refraction via quantum coherence. *Physical Review Letters* **67**, 1855–1858 (1991).
46. Fleischhauer, M. *et al*. Resonantly enhanced refractive index without absorption via atomic coherence. *Physical Review A* **46**, 1468–1487 (1992).
47. Zibrov, A. S. *et al*. Experimental Demonstration of Enhanced Index of Refraction via Quantum Coherence in Rb. *Physical Review Letters* **76**, 3935–3938 (1996).
48. Yavuz, D. D. Refractive Index Enhancement in a Far-Off Resonant Atomic System. *Physical Review Letters* **95**, 223601 (2005).
49. Proite, N. A., Unks, B. E., Green, J. T. & Yavuz, D. D. Refractive Index Enhancement with Vanishing Absorption in an Atomic Vapor. *Physical Review Letters* **101**, 147401 (2008).
50. Dridi, K., Benhsaien, A., Zhang, J., Hinzer, K. & Hall, T. J. Narrow linewidth two-electrode 1560 nm laterally coupled distributed feedback lasers with third-order surface etched gratings. *Opt. Express* **22**, 11 (2014).
51. Gao, F. *et al*. Study of gain-coupled distributed feedback laser based on high order surface gain-coupled gratings. *Optics Communications* **410**, 936–940 (2018).
52. Liu, Y.-M., Gao, F., Fan, C.-H. & Wu, J.-H. Asymmetric light diffraction of an atomic grating with PT symmetry. *Opt. Lett.* **42**, 4283–4286 (2017).
53. Shui, T., Yang, W.-X., Liu, S., Li, L. & Zhu, Z. Asymmetric diffraction by atomic gratings with optical PT symmetry in the Raman-Nath regime. *Physical Review A* **97**, 033819 (2018).

Acknowledgements

This work was supported by National Natural Science Foundation of China (61774156 and 61761136009), External Cooperation Program of Chinese Academy of Sciences (181722KYSB20160005), Jilin Provincial Natural Science Foundation (20160520095JH and 20180519024JH), the program of China Scholarships Council (201604910385) and the Youth Innovation Promotion Association of Chinese Academy of Sciences (2018249).

Author Contributions

S.-C.T. proposed the research and carried out the calculations. R.-G.W. verified the results. All authors discussed the results and reviewed the manuscript.

Additional Information

Competing Interests: The authors declare no competing interests.

Publisher's note: Springer Nature remains neutral with regard to jurisdictional claims in published maps and institutional affiliations.